Stabilisation of the Hydrodynamic Instability by the Critical Layer

Doi: 10.2514/6.2022-3096

Matthew J. King* and Edward J. Brambley†
Mathematics Institute, University of Warwick, Coventry CV4 7AL, UK
WMG, University of Warwick, Coventry CV4 7AL, UK

Acoustics are considered in a straight cylindrical duct with an axial mean flow that is uniform apart from a boundary layer near the wall. Within the boundary layer, which may or may not be thin, the flow follows a quadratic curve to satisfy no-slip at the wall. Modal solutions to the linearised Euler equations are found by solving the Pridmore-Brown equation using Frobenius series. The modes usually identified as Hydrodynamic Instabilities are found to interact with the critical layer branch cut, also known as the continuous spectrum. By varying the boundary layer thickness, flow speed, frequency and impedance, it is found that the instabilities can be stabilised behind the critical layer branch cut. In these cases, the effect of these (now stable) modes is included within the critical layer non-modal contribution, and may be the dominant downstream effect; this is found to be particularly true for sound sources located near the wall.

I. Introduction

Acoustic linings are typically modelled as an impedance boundary condition at a duct wall. It is well known that a mean flow that does not satisfy no-slip at the wall, such as a uniform flow, complicates the impedance boundary condition. The often-used Ingard–Myers [1] boundary condition is illposed [2], leading to both numerical and theoretical difficulties, and does not match well with experimental observations [e.g. 3]. It may be regularized by allowing for a thin boundary layer over the wall [4]; while this regularized boundary condition also leads to a significant increase in accuracy when solving the linearized Euler equations [5], it too does not accurately reproduce experimental observations [6]. Various attempts have been made at improved impedance boundary conditions [e.g. 7–9], but to date no impedance boundary condition matches well with experimental observations [10, 11]. The alternative is to include a varying mean flow which satisfies the no-slip condition at the duct wall. This, however, introduces its own complications, including the critical layer, otherwise known as the continuous spectrum [12].

Most investigations of the interaction of sound and acoustic linings consider the duct modes in the frequency domain. A reasonably general solution is then given as linear sum of these modes, with amplitudes fitted to emulate a particular sound source. This is the basis of techniques such as mode-matching [e.g. 13, 14]. Modes also occur as poles in complex analytic methods, such as the the Weiner-Hopf technique [e.g. 15–17]. One complication of considering duct modes in the frequency domain is determining their direction of propagation; this can be achieved using the Briggs–Bers criterion [18, 19]. Most modes are stable and decay in their direction of propagation, but a number of surface wave modes exist with interesting properties [20, 21], and one such surface wave mode is thought to be a hydrodynamic instability. There is also some experimental evidence of instabilities [e.g. 22], although the hydrodynamic instability is in most cases the least well theoretically-predicted duct mode using the various impedance boundary conditions.

When considering a non-uniform mean flow in the frequency-domain, the pressure perturbation is governed by the Pridmore-Brown equation [23]. Since the Pridmore-Brown equation is not self-adjoint, the duct modes are not necessarily complete, and so a general solution cannot necessarily be described as just a sum of duct modes. This difficulty manifests itself as the critical layer. Solving analytically for the Greens function for a point mass source in a duct, the Greens function is found to consist not only of a sum of modes, but also includes a Fourier inversion integral around the critical layer [12, 24]. This results in an extra term in the solution downstream of the point mass source, including a neutrally stable non-decaying term if the source is located in any region of non-constant mean flow [12, 24, 25]. Despite this, the critical layer is often ignored, either explicitly or implicitly, with its contribution argued to be small compared to that of the sum of duct modes, with some justification [12].

*PhD, Mathematics Institute, Univeristy of Warwick. AIAA student member.
†Associate Professor, Mathematics Institute & WMG, University of Warwick. Senior AIAA Member.

Whatever the effect of the critical layer, it is dominated in the far-field downstream of the source by any hydrodynamic instability. However, it was found [21] that the hydrodynamic instability could move behind the critical layer branch cut for certain boundary layer profiles and parameters; this then resulted in a stable situation. However, this was not investigated further due to the numerical method being unable to track the hydrodynamically unstable surface wave mode behind the critical layer. The Frobenious method [12] is capable of tracking the mode behind the branch cut, but, for the linear boundary layer flow profile used in that case, the hydrodynamic instability mode never went behind the branch cut. However, more recently, the Frobenious method has been used to analyse a quadratic boundary layer profile [24], and the hydrodynamic instability is found to move behind the critical layer branch cut in this case. In this case, it was found that not only was the solution then stable, but that the contribution of this hidden pole was included in the Fourier inversion integral around the critical layer, meaning that this pole could still be dominant in the far-field, particularly for a sound source close to the wall; in this case, ignoring the critical layer would give inaccurate results.

In this work, we will examine the stabilization of the hydrodynamic instability as it interacts with and moves behind the critical layer. In particular, we will observe the effects on this behaviour of frequency, impedance, and boundary layer thickness. In section II we summarise the Frobenious solutions from King et al. [24]. Using the code provided alongside King et al. [24], a parameter study is performed in section III. This allows us to find the critical boundary layer thickness that leads to the stabilization of the hydrodynamic 'instability'.

II. Formulation and Solutions to the Pridmore-Brown Equation

The governing equations for what follows are the Euler equations in cylindrical co-ordinates,

$$\frac{\partial \rho}{\partial t}+\frac{\partial(\rho u_x)}{\partial x}+\frac{1}{r}\frac{\partial(r\rho u_r)}{\partial r}+\frac{1}{r}\frac{\partial(\rho u_\theta)}{\partial \theta}=0, \qquad \frac{Dp}{Dt}=c^2\frac{D\rho}{Dt}, \tag{1}$$
$$\rho\frac{Du_x}{Dt}=-\frac{\partial p}{\partial x}, \qquad \rho\frac{Du_r}{Dt}-\frac{1}{r}\rho u_\theta^2=-\frac{\partial p}{\partial r}, \qquad \rho\frac{Du_\theta}{Dt}+\frac{1}{r}\rho u_r u_\theta=-\frac{1}{r}\frac{\partial p}{\partial \theta}.$$

We write each variable as a steady mean flow plus a small time-harmonic perturbation of order ϵ and frequency ω,

$$\rho=\rho_0(r)+\mathrm{Re}\left(\epsilon\hat{\rho}e^{\mathrm{i}\omega t}\right)+O(\epsilon^2), \qquad p=p_0+\mathrm{Re}\left(\epsilon\hat{p}e^{\mathrm{i}\omega t}\right)+O(\epsilon^2),$$
$$\boldsymbol{u}=(u_x,u_r,u_\theta)=U(r)\boldsymbol{e_x}+\mathrm{Re}\left(\epsilon(\hat{u},\hat{v},\hat{w})e^{\mathrm{i}\omega t}\right)+O(\epsilon^2), \qquad c^2=c_0^2(r)+O(\epsilon), \tag{2}$$

where p_0 is necessarily a constant in order that the steady state should satisfy the Euler equations. All perturbations are then expanded using a Fourier series in θ and a Fourier transform in x. As a result, the pressure perturbation is given as

$$\hat{p}(x,r,\theta)=\frac{1}{2\pi}\sum_{m=-\infty}^{\infty}\mathrm{e}^{-\mathrm{i}m\theta}\int_{-\infty}^{\infty}\widetilde{p}(r;k,m,\omega)\mathrm{e}^{-\mathrm{i}kx}\,\mathrm{d}k, \tag{3}$$

and similarly for the density $\hat{\rho}$ and the velocity components $\hat{u}$, $\hat{v}$ and $\hat{w}$. Ignoring terms of order $O(\epsilon^2)$ and solving the Euler equations (1) for the pressure perturbation gives

$$\widetilde{p}''+\left(\frac{2kU'}{\omega-U(r)k}+\frac{1}{r}-\frac{\rho_0'}{\rho_0}\right)\widetilde{p}'+\left(\frac{(\omega-U(r)k)^2}{c_0^2}-k^2-\frac{m^2}{r^2}\right)\widetilde{p}=0 \tag{4a}$$

$$\text{with} \qquad \tilde{v}=\frac{\mathrm{i}\widetilde{p}'}{\rho_0(\omega-Uk)}, \tag{4b}$$

where a prime denotes the derivative with respect to r. Equation (4a) is the Pridmore-Brown equation [23].

Here, for simplicity, we assume a constant mean density $\rho_0(r)$, meaning that the flow is homentropic, and resulting in a constant speed of sound $c_0(r)=c_0$. We also choose a flow profile $U(r)$ that is uniform except within a boundary layer of width h, where it varies quadratically:

$$U(r)=\begin{cases}c_0M & 0\le r\le 1-h\\ c_0M(1-(1-\frac{1-r}{h})^2) & 1-h\le r\le 1\end{cases}. \tag{5}$$

Here M is the centreline Mach number. Note that we do not assume that the boundary layer is thin, so h need not be small. This situation is represented schematically in figure 1.

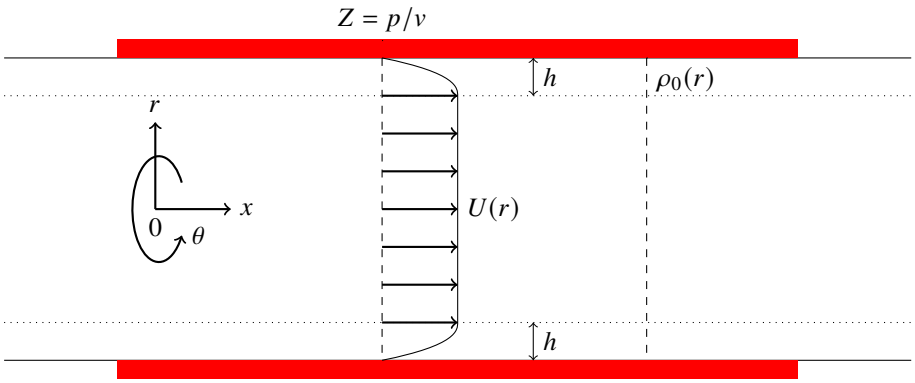

Fig. 1 Schematic of a cylindrical duct with lined walls containing sheared axial flow. $\rho_0(r)$ is the mean flow density (here taken constant), and $U(r)$ is the mean flow velocity, here taken to be uniform outside a boundary layer of width h. Z is the boundary impedance and defines the boundary condition at the wall of the duct.

We non-dimensionalize speeds by the sound speed c_0, densities by ρ_0, and distances by the duct radius a. Under these assumptions and non-dimensionalizations, the Pridmore-Brown equation (4a) reduces to

$$\widetilde{p}'' + \left(\frac{2kU'}{\omega - U(r)k} + \frac{1}{r}\right)\widetilde{p}' + \left((\omega - U(r)k)^2 - k^2 - \frac{m^2}{r^2}\right)\widetilde{p} = 0. \tag{6}$$

We require the solution to be regular at the centreline $r = 0$, and to satisfy an impedance boundary condition at the duct wall $r = 1$. Since our mean flow is nonslipping, $U(1) = 0$, this is given by

$$\widetilde{p}(1) = Z(\omega)\tilde{v}(1), \qquad \text{or equivalently} \qquad \widetilde{p}'(1) - \frac{\mathrm{i}\omega}{Z}\widetilde{p}(1) = 0, \tag{7}$$

where $Z(\omega)$ is the impedance of the duct wall, and a hard wall corresponds to $Z \to \infty$.

In [24], the Pridmore-Brown equation with this constant-then-quadratic flow profile is solved using a Frobenius method. These solutions are then used to construct a Greens function solution for the inhomogeneous Pridmore-Brown equation, and the Fourier inversion is found. This was used to explore the non-modal contribution of the critical layer. Here, we will use the same Frobenius solutions to find the modes of (6). The important features of the solutions from [24] used here are now breifly summarised.

A. Frobenius Solution to the Pridmore-Brown Equation

The Pridmore-Brown equation (6) can be split into two cases according to if we are within the uniform or sheared flow regions (5). When $r < 1 - h$, we are in the uniform flow region, and

$$\widetilde{p}'' + \frac{1}{r}\widetilde{p}' + \left((\omega - Mk)^2 - k^2 - \frac{m^2}{r^2}\right)\widetilde{p} = 0, \tag{8}$$

with solutions in terms of Bessel function of order m. Requiring regularity at $r = 0$, this gives the solution in the uniform flow region as

$$\widetilde{p}(r) = J_m(\alpha r) \qquad \text{with } \alpha^2 = (\omega - Mk)^2 - k^2. \tag{9}$$

In contrast, when $r > 1 - h$, we are in the sheared flow region, and, for this quadratic flow profile, the Pridmore-Brown equation (6) can be written as

$$\widetilde{p}'' + \left(\frac{1}{r} - \frac{2}{r - r_c^-} - \frac{2}{r - r_c^+}\right)\widetilde{p}' + \left(\frac{M^2k^2}{h^4}(r - r_c^+)^2(r - r_c^-)^2 - k^2 - \frac{m^2}{r^2}\right)\widetilde{p} = 0, \tag{10}$$

where $r_c^\pm$ are the locations of the critical layer, given by $\omega - U(r_c)k = 0$. Since $U(r)$ is quadratic for $r > 1 - h$, this is a quadratic equation to solve, with two solutions,

$$r_c^\pm = 1 - h \pm h\sqrt{1 - \frac{\omega}{Mk}}. \tag{11}$$

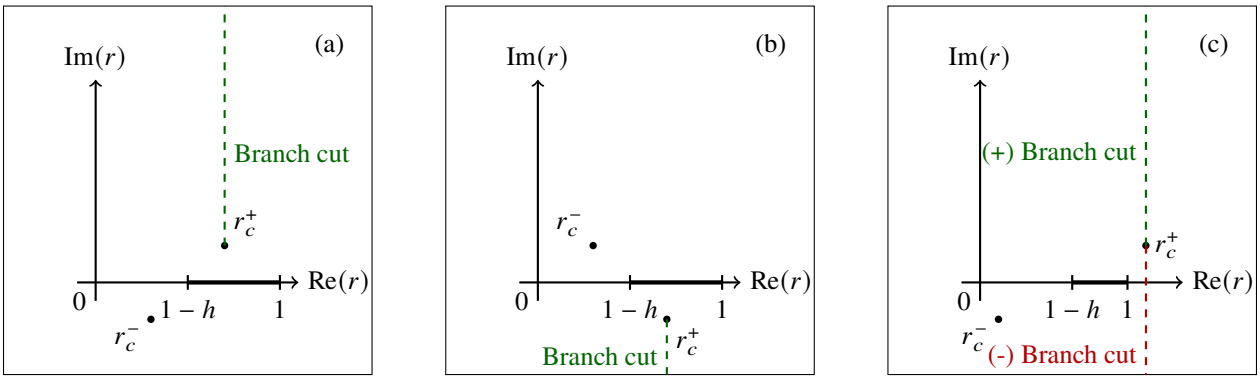

Fig. 2 Schemetic of possible locations of the r_c^+ branch cut in the complex r-plane. (a) A possible choice of branch cut when $\mathrm{Im}(r_c^+) > 0$ and $\mathrm{Re}(r_c^+) < 1$. (b) Branch cut choice when $\mathrm{Im}(r_c^+) < 0$ and $\mathrm{Re}(r_c^+) < 1$. (c) When $\mathrm{Re}(r_c^+) > 1$ we can choose which branch cut to consider.

We choose $\mathrm{Re}(\sqrt{\cdots}) \geq 0$, so that $\mathrm{Re}(r_c^+) \geq 1 - h$; it will turn out that r_c^+ is the root we will be most interested in throughout. As in [24], equation (10) can be solved using Frobenius series expansion about r_c^+, resulting in two linearly independent solutions

$$\widetilde{p}_1(r) = \sum_{n=0}^{\infty} a_n (r - r_c^+)^{n+3}, \qquad \widetilde{p}_2(r) = A\widetilde{p}_1(r)\log(r - r_c^+) + \sum_{n=0}^{\infty} b_n (r - r_c^+)^n, \tag{12a}$$

$$\text{where } a_0 = b_0 = 1 \qquad \text{and} \quad A = -\frac{1}{3}\left(\frac{1}{r_c^+ - 1 + h} - \frac{1}{r_c^+}\right)\left(k^2 + \left(\frac{m}{r_c^+}\right)^2\right) - \frac{2m^2}{3r_c^{+3}}, \tag{12b}$$

and the a_n and b_n coefficients are given by a recurrence relation in [24]. While the specifics of these solutions are omitted here, we comment that matlab code is provided in [24] to compute these solutions.

To solve the Pridmore-Brown equation across the whole of $r \in [0, 1]$, the two types of solutions above are spliced together such that the resulting solution and its derivative are continuous at $r = 1 - h$:

$$\widetilde{p}(r) = \begin{cases} J_m(\alpha r) & 0 \leq r \leq 1 - h \\ C_1\widetilde{p}_1(r) + D_1\widetilde{p}_2(r) & 1 - h \leq r \leq 1, \end{cases} \tag{13}$$

with C_1 and C_2 chosen to ensure continuity of $\widetilde{p}$ and $\widetilde{p}'$ at $r = 1 - h$.

In general, $\widetilde{p}(r)$ does not satisfy the impedance boundary condition (7) at $r = 1$. We therefore search for modal solutions by varying k such that $\widetilde{p}(r)$ does satisfy the impedance boundary condition (7) at $r = 1$. This is performed using the matlab code from [24], which uses a variant of the Secant method, and has been verified against finite-difference solutions to the Pridmore-Brown equation. The major advantage of using this method is its treatment of the critical layer branch cut.

B. The Critical Layer Branch Cut

The most important detail of the solution method used here is the presence of the log term in (12). The branch of log should clearly be chosen to maintain a continuous solution for $\widetilde{p}_2(r)$, and hence $\widetilde{p}(r)$, along $r \in [1 - h, 1]$. The direction of the resulting branch cuts is illustrated in figure 2. The only difficulty is when $\mathrm{Im}(r_c^+) = 0$, and indeed $\mathrm{Im}(r_c^+) \to 0$ from below or from above gives different solutions. We therefore exclude values of k for which $\mathrm{Im}(r_c^+) = 0$ and $\mathrm{Re}(r_c^+) \in [1 - h, 1]$. This results in a branch cut in the complex k plane along the real half line $[\frac{\omega}{M}, \infty)$. We refer to the branch cut in the complex k plane as the critical layer branch cut; this range is also sometimes referred to as the continuous spectrum.

One of the major advantages of the Frobenius method used here is that we are free to choose the branch of log, and so we may in effect analytically continue behind the critical layer branch cut. In so doing, we are able to find any modes that are hidden behind the branch cut. This has two important uses. The first is that modes behind the critical layer

Table 1 Parameter Set Values.

		A1	A2	B1	B2
Frequency	ω	31	31	10	10
Centre line Mach Number	M	0.5	0.5	0.5	0.5
Azimuthal order	m	24	24	24	24
Boundary layer thickness	h	0.01	0.005	0.005	0.005
Impedance Mass	μ	0.01	0.01	0.06	0.1
Impedance Spring	K	10	10	3	5
Impedance Damper	R	0.75	0.75	0.75	0.75
Impedance	$Z(\omega)$	$0.75 - 0.0126\mathrm{i}$	$0.75 - 0.0126\mathrm{i}$	$0.75 + 0.3\mathrm{i}$	$0.75 + 0.5\mathrm{i}$

branch cut do still contribute to the pressure perturbation $\hat{p}(x, r, \theta)$, though they do so as a Fourier inversion integral around the critial layer branch cut, rather than as an individual mode in its own right; see [24] for details. Secondly, modes behind the critical layer branch cut can move across the branch cut and become legitimate modes in the usual sense as parameters are varied, and we will see later that, as the boundary layer thickness h is reduced, a mode emerges from the critical layer branch cut and becomes a hydrodynamic instability.

III. Parameter Studies of the Hydrodynamic 'Instability'

Throughout the following sections we will make use the parameter sets given in table 1. These parameters have been chosen deliberately to demonstrate a variety of behaviours as the parameters are varied, particularly focusing on the stabilisation of the hydrodynamic instability pole. In figure 3 the pole locations for each parameter set are shown, with an indication of which poles are stable or unstable. Throughout this section, we will refer to the hydrodynamic instability mode as k_{HI}, whether or not it is actually unstable.

In section III.A we will investigate how the hydrodynamic instability is stabilised in the boundary layer thickness h, drawing attention to the threshold value h_c that leads to neutral stability. Following this, in III.B we will make use of our ability to find h_c to observe how the stability depends on each of the parameters. Finally in III.C we compare the behaviour seen here to those of a linearly sheared flow profile.

A. The effect of boundary layer thickness.

Figure 3 shows a hydrodynamic instability in the upper-right k-plane for parameter set A2, but not for parameter set A1. As the only difference between A1 and A2 is the boundary layer thickness, this illustrates that increasing the boundary layer thickness can stabilize the hydrodynamic instability. Figure 4 tracks how the modal solutions move in the k-plane as the boundary layer thickness h is varied. From figure 4(A), it can be seen that the hydrodynamic instability in A2 stabilizes by crossing the critical layer branch cut as h is increased. By using the Frobenius method to find modes, we are here able to continue tracking the mode behind the critical layer branch cut as h continues to increase.

A similar situation is shown in each case in figure 4; in each case, increasing the boundary layer thickness leads to a stable flow. Moreover, as $h \to 1$, the k_{HI} mode approaches the branch point located at $k = \omega/M$ from behind the branch cut. Comparing parameters sets $B1$ and $B2$, both with potentially two k_{HI} modes, only one is found to be an instability, and in both cases as the boundary layer is thickened the instability is stabilized, while the other mode becomes a standard cut-off mode. We will later observe that, when varying the impedence Z, the two modes are related.

From the results shown here, it appears that the hydrodynamic instability is stabilized by the critical layer branch cut provided the boundary layer is sufficiently thick. In what follows, we define a critical boundary layer thickness h_c for which the k_{HI} mode is located exactly on the critical layer branch cut. As such, the k_{HI} mode is stable for $h > h_c$, and is unstable for $h < h_c$. We calculate h_c here numerically by tracking the location of the k_{HI} mode as the boundary layer thickness is varied, seeking smaller imaginary parts until a real value is achieved.

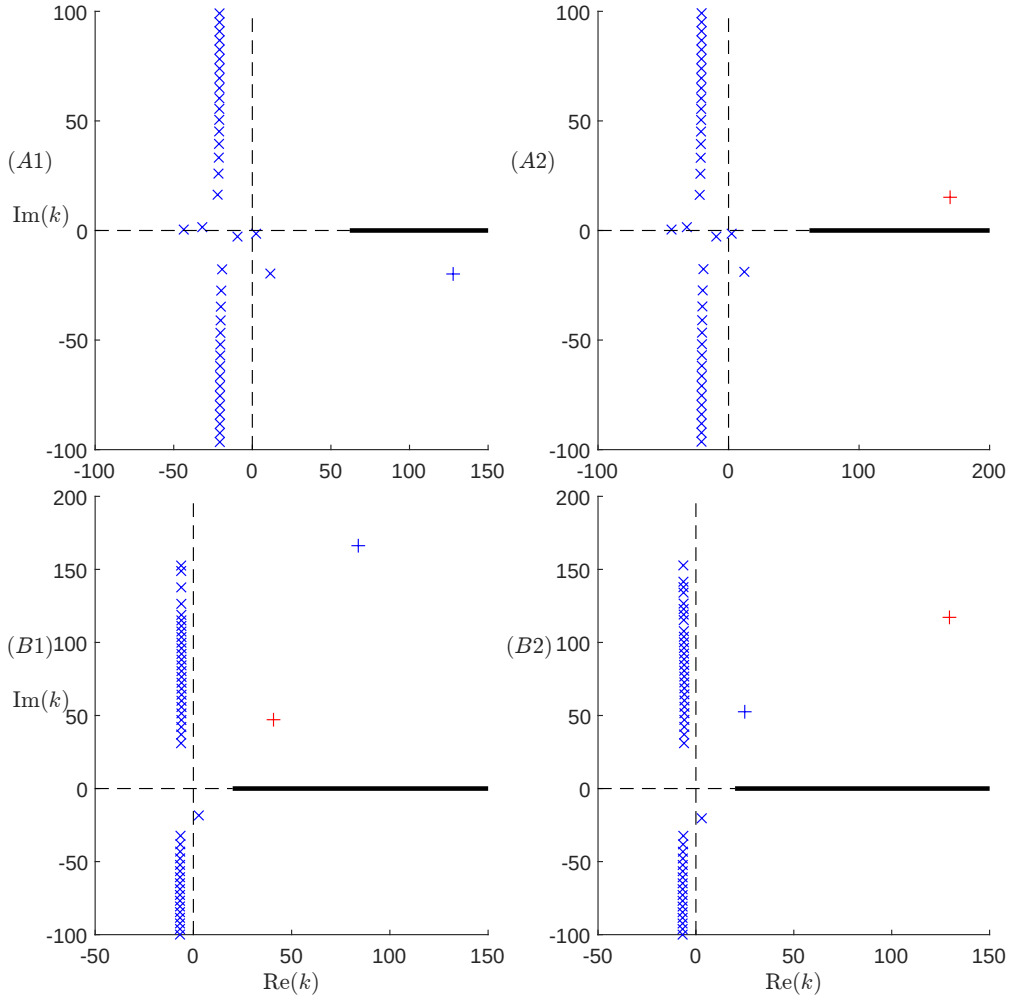

Fig. 3 Locations in the complex k plane of modal solutions for each of the four parameter sets listed in table 1. Stable modes are indicated in blue. Unstable modes are coloured red. The hydrodynamic instability is marked with a plus (+), while all other modes are marked with a (×). The critical layer branch cut is indicated with by the thick black line.

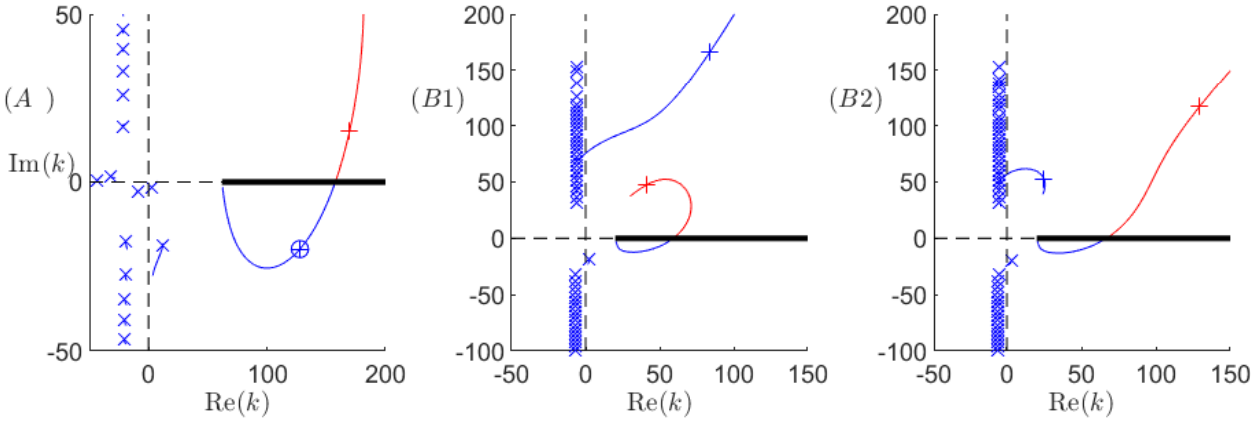

Fig. 4 Location in the complex k plane of modal solutions as the boundary layer thickness is varied, for the parameter sets listed in table 1. The boundary layer thickness h ranges from 0.1 to 5×10^{-4}. The hydrodynamic instability mode for parameter set $A1$ has been circled.

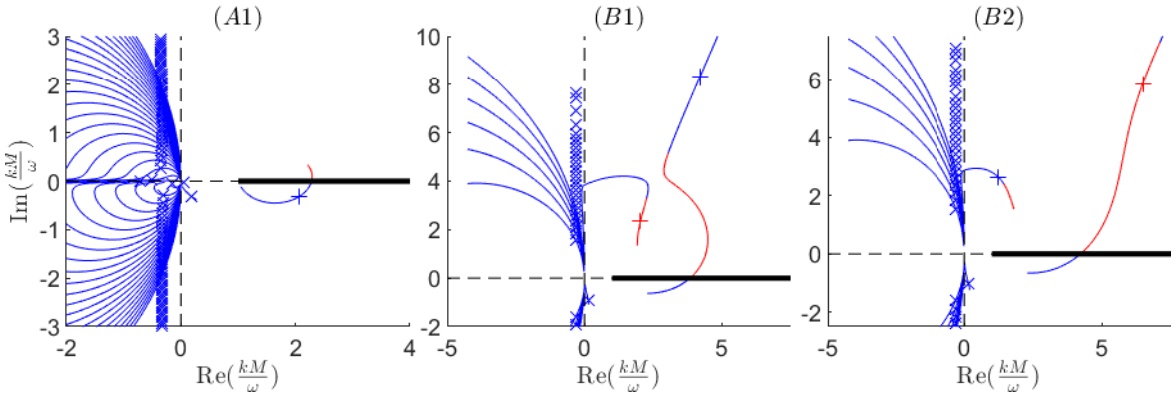

Fig. 5 Movement of the modal solutions in the complex k plane as the Mach number is varied from 0.1 to 0.9, for parameter sets A1, B1 and B2 given in table 1. The axes have been scaled by M/ω in order to keep the location of the critical layer branch cut fixed.

B. Varying the parameters

Figure 5 shows the results of varying the Mach number M. In order to keep the critical layer fixes as the Mach number is varied, note that a scaled k-plane is used. Figure 5 shows that, as the Mach number is decreased while keeping the boundary layer fixed, the flow is stabilised. At the same time, for lower flow speeds there are fewer cut-on modes, and as $M \to 0$ the modes approach their no-flow equivalents, as expected. When there are two candidate k_{HI} modes, again we find that only one of them may be unstable, although as the Mach number is varied which one is unstable may change.

Figure 6 shows how h_c and $k_{\mathrm{HI}}(h_c)$ vary as the Mach number is varied. As expected from figure 5, we observe that h_c increases as the Mach number is increased. This appears to follow a remarkably linear trend, with a gradient depending on the other parameters. We note, however, that numerically it becomes increasingly difficult to track the value of h_c for small Mach numbers, as k_{HI} becomes increasingly large for small M.

Similarly, we may vary the frequency ω, as shown in figures 7 and 8. It can be observed that a hydrodynamic instability may be present only for a range of intermediate frequencies, with high and low frequencies being stable for a thinner boundary layer thicknesses. It is also possible that a sufficiently large boundary layer thickness can be stability for all frequencies, as is the case for parameter set $A1$ here. This could be of particular importance for broadband time domain simulations.

Figures 9 and 10 show the effect of varying the impeance Z. In figure 9 we only track the location of the modes as $\mathrm{Im}(Z)$ is varied, while figure 10 gives a contour plot of the variation of h_c and $k_{\mathrm{HI}}(h_c)$ as both real and imaginary parts of Z are varied. This contour plot is limited for large $|Z|$ due to numerical accuracy, as once again the value of $k_{\mathrm{HI}}(h_c)$ becomes too large. However, we may still conclude that, as $|Z| \to \infty$ and the duct becomes hard walled, the flow is stable for any finite thickness boundary layer. This is observed in figure 9 by looking at the pole location in both hard wall limits, $\mathrm{Im}(Z) \to \pm\infty$, indicated with a triangle, and in figure 10 by observing that h_c is decreasing as $|Z|$ becomes larger.

The impedance Z is usually a function of frequency ω, and when the frequency ω has been varied above we have assumed a mass–spring–damper impedance $Z(\omega) = R + \mathrm{i}(\mu\omega - K/\omega)$, with parameters given in table 1: in particular, this means that for large and small values of ω we have $\mathrm{Im}(Z(\omega)) \to \pm\infty$. It is therefore also worth considering how the combination of varying the frequency and the impedance model together affects the overall behaviour of the system. To this end, figure 11 illustrates the value of h_c as the impedance, mass, spring and damper terms are varied alongside the frequency. From these graphs two different behaviours may be observed. Firstly, when varying either the impedance mass or spring coefficient, if we choose to maintain a constant impedance, as indicated in figure 11 by the dashed lines, as we increase the frequency we do indeed observe a stabilising effect; that is, as ω is increased, h_c decreases. However we appear to observe a destabilization as the frequency is decreased at fixed impedance, suggesting that our stabilisation when considering low frequencies is due to the resulting impedance having a large negative imaginary part, and therefore being spring-like. A second observation is that for a fixed frequency, the impedance giving the most stability (i.e. with the largest h_c), is close to, but not exactly equal to, the optimal damping frequency $\omega = \sqrt{K/\mu}$ when we have a small damping coefficient. Moreover, the frequency with the largest value of h_c has a significant dependence

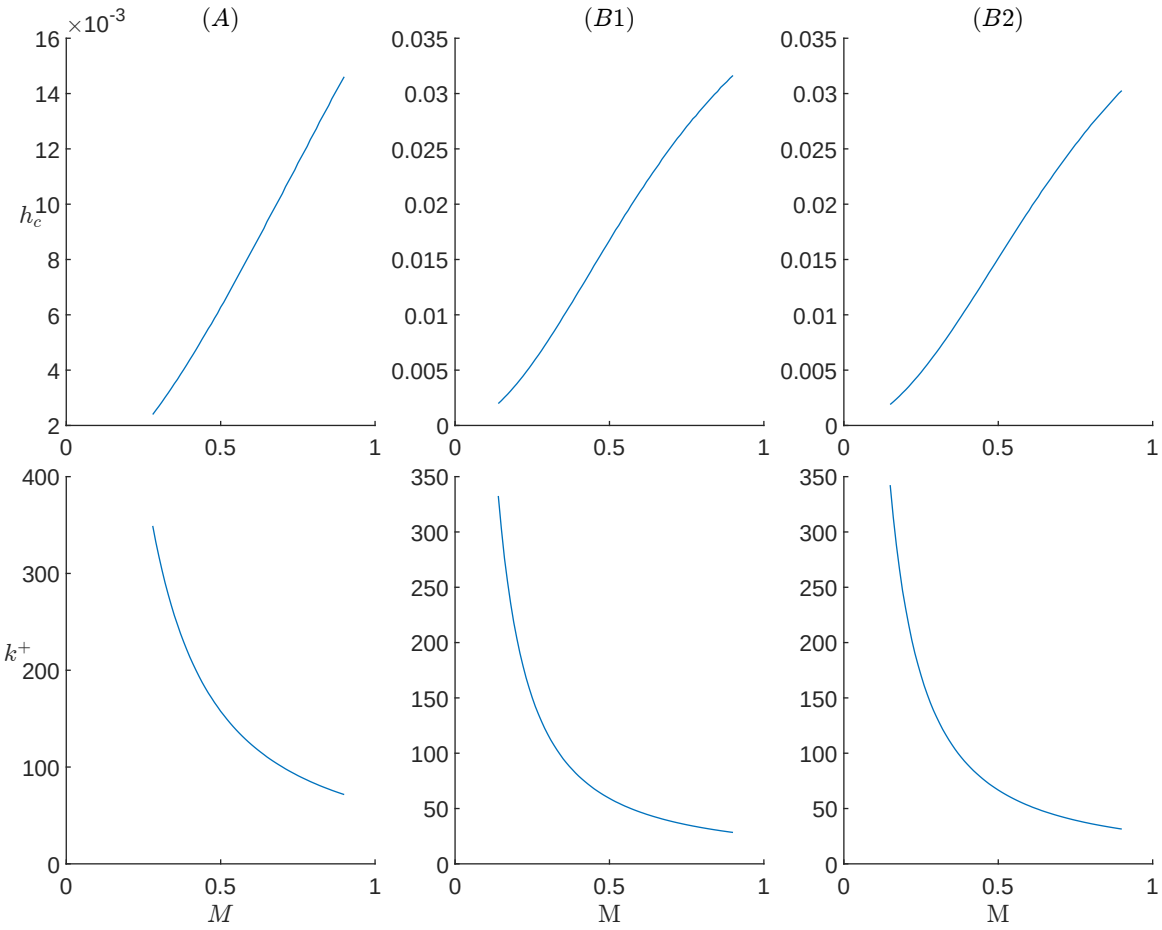

Fig. 6 (Top) Value of h_c plotted as the Mach number is varied. (Bottom) Value of $k(h_c)$ for the hydrodynamic instability as the Mach number is varied. Figures have been plotted for each parameter set listed in table 1; note that A1 and A2 only differ in boundary layer thickness and therefore result in the same plot, labelled (A) here.

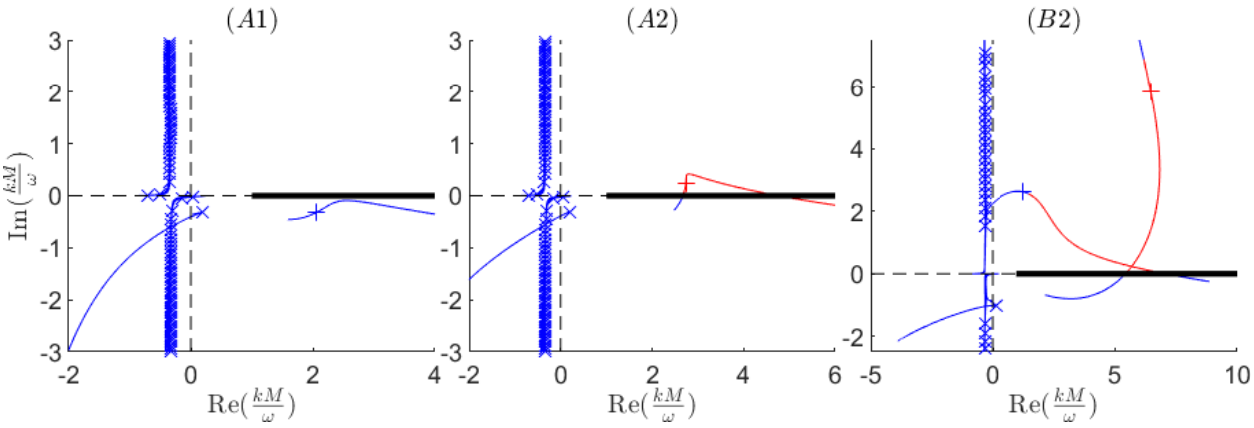

Fig. 7 As for figure 5, but for varying frequency ω from 1 to 50. Note that $Z(\omega)$ varies as ω is varied.

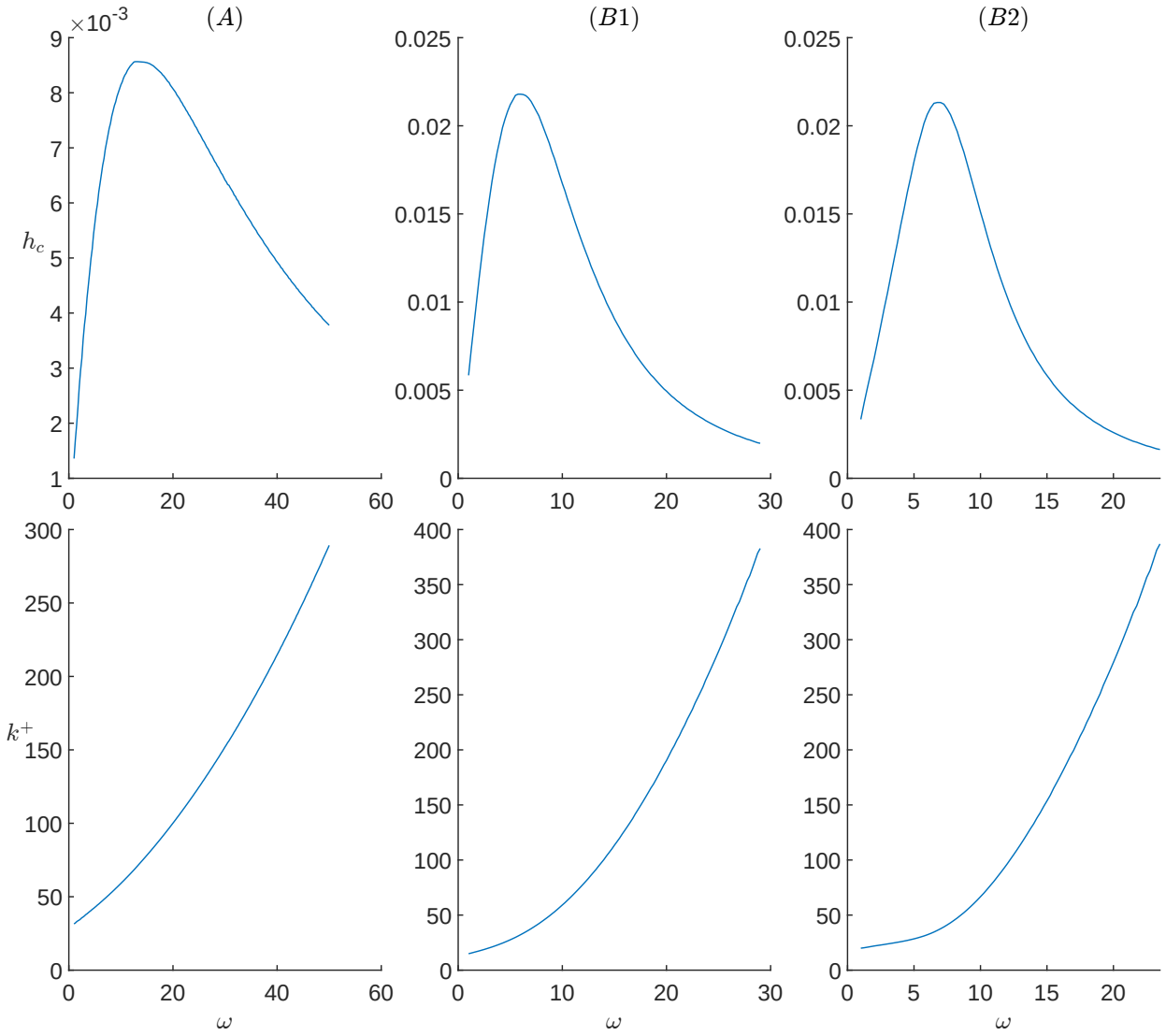

Fig. 8 As figure 6, but for varying the frequency.

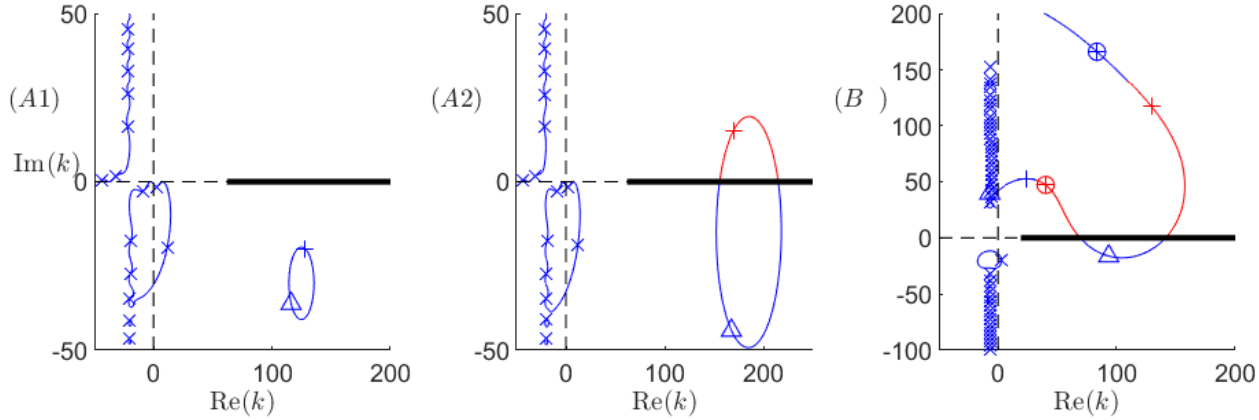

Fig. 9 Locations of the modal solutions in the complex k-plane as the reactance, $\mathrm{Im}(Z)$, is varied from $-\infty$ to ∞. The hydrodynamic instability for $|Z| = \infty$ is indicated by a triangle ($\triangle$). The hydrodynamic instability for parameter set B1 is circled.

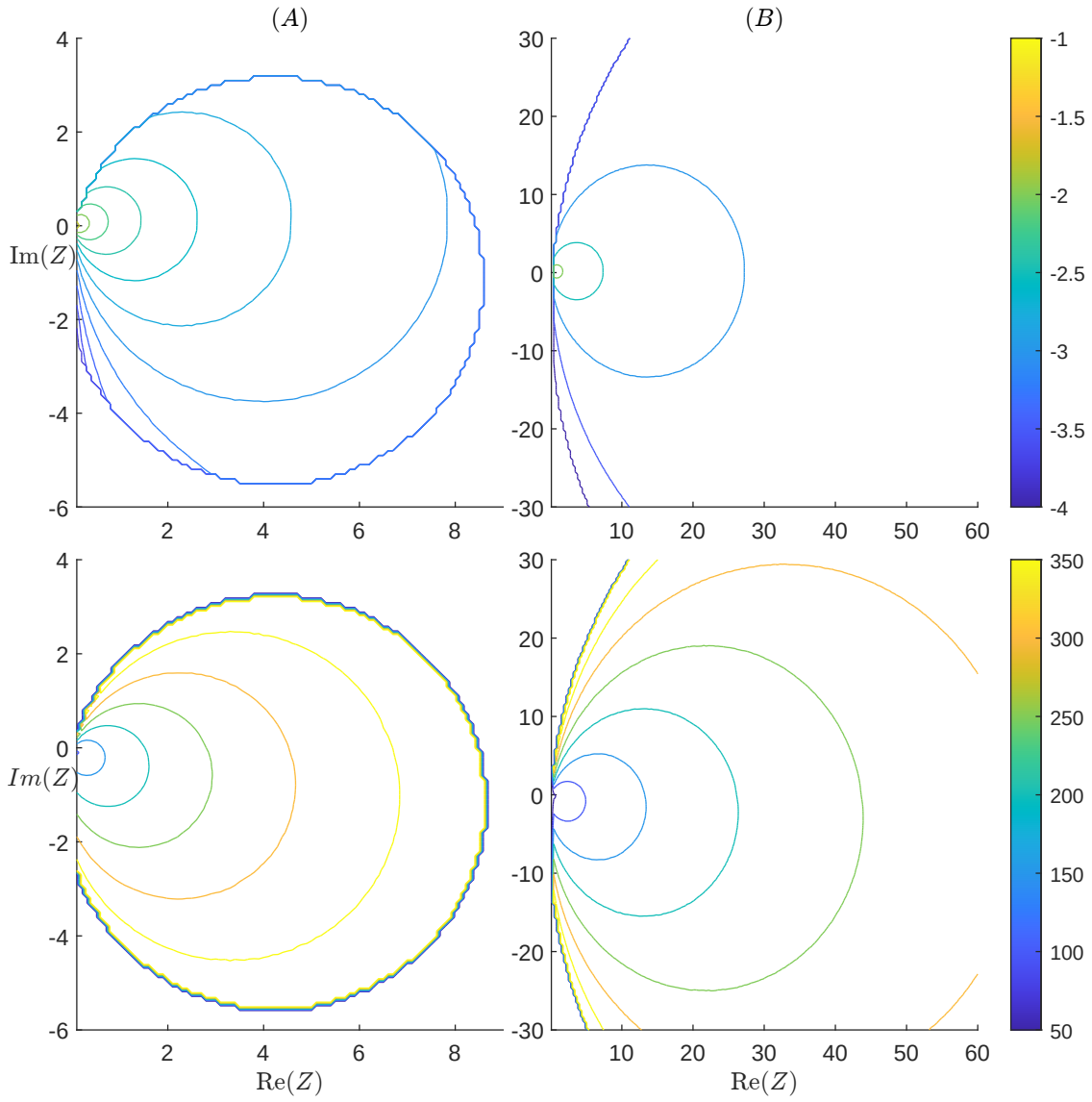

Fig. 10 Contour plot of h_c (left) and $k(h_c)$ against $\mathrm{Re}(Z)$ and $\mathrm{Im}(Z)$. Values of h_c are indicated on a $\log_{10}$ scale. The large wrinkled outer circle denotes the limits of numerical resolution.

on the damping coefficient, although their relationship is not clear. This observation is made by noting the peaks of h_c are near the dashed line representing $\mathrm{Im}(Z) = 0$ in both the impedance mass and spring graphs, while this is only true in the impedance damper graph for small damping coefficients. Note that $R = 0.75$ in both parameter sets A and B when taken to be fixed.

C. Comparison to a Linear Shear flow profile

The Frobenius solution used here to track the pole locations is specific to a quadratic shear flow profile. However, a similar Frobenius expansion exists for a linear flow profile [12]. We may therefore repeat the analysis above to compare the quadratic and linear boundary layer profiles, and a significant difference is seen. This is done in figures 12-15 for the boundary layer thickness, Mach number, frequency, and impedance. In each of these it can be observed that the linear flow profile is unstable for all boundary layer thicknesses, and so the hydrodynamic instability will always be present. There is some similarity, however, and for cases where stability was found for the quadratic shear, in the linear case we instead have a hydrodynamic instability with a small imaginary part. As a result of this, the growth rate of the pole

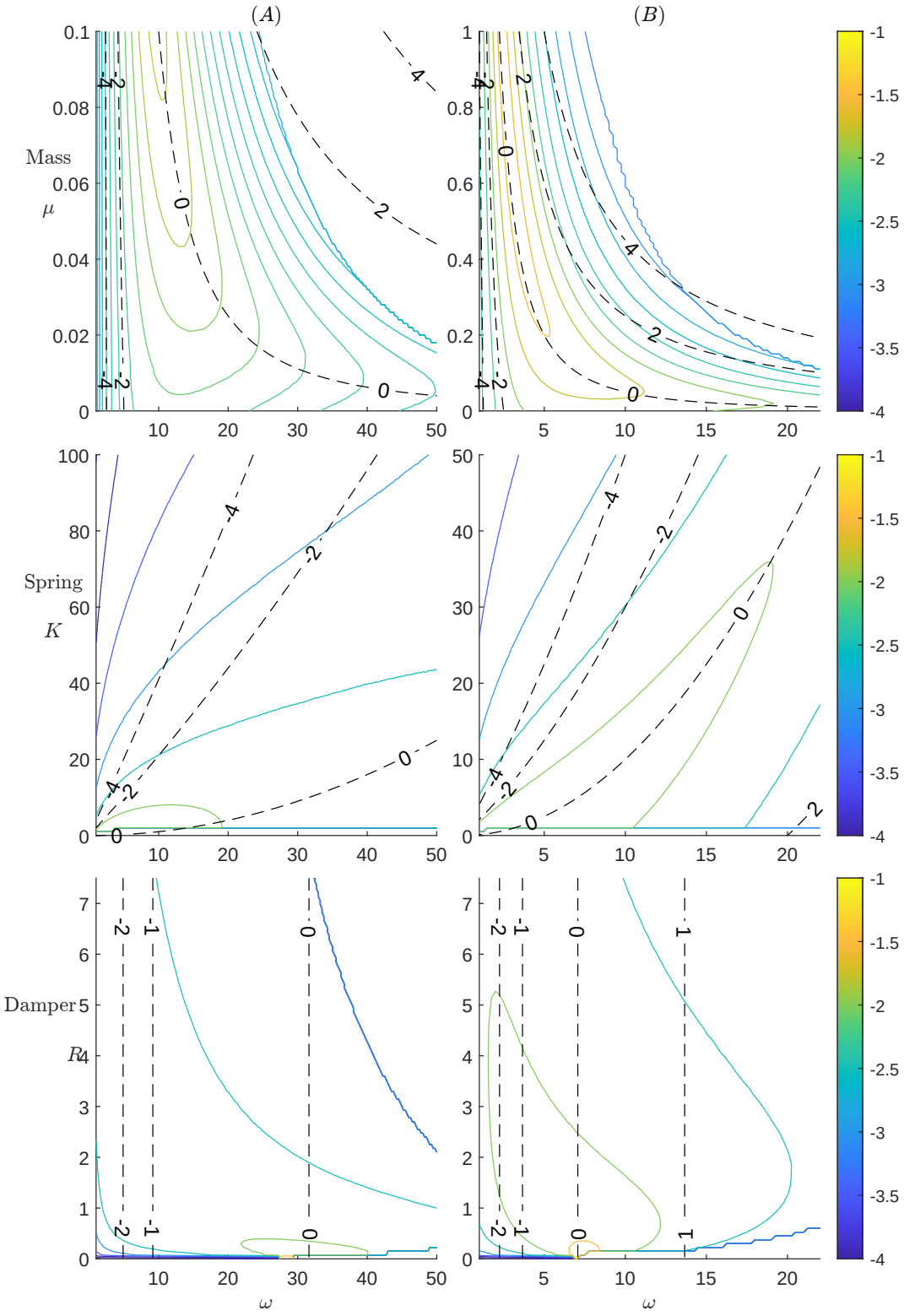

Fig. 11 Contour plots of h_c (on a $\log_{10}$ scale) as the frequency and impedance are varied, performed for Parameter Set A and B, with the impedance mass, spring and damper terms being varied between 0 and 10 times their original value. Black dashed lines $(--)$ indicate lines of constant impedance $Z = Z(\omega)$ with the value of $\mathrm{Im}(Z)$ indicated.

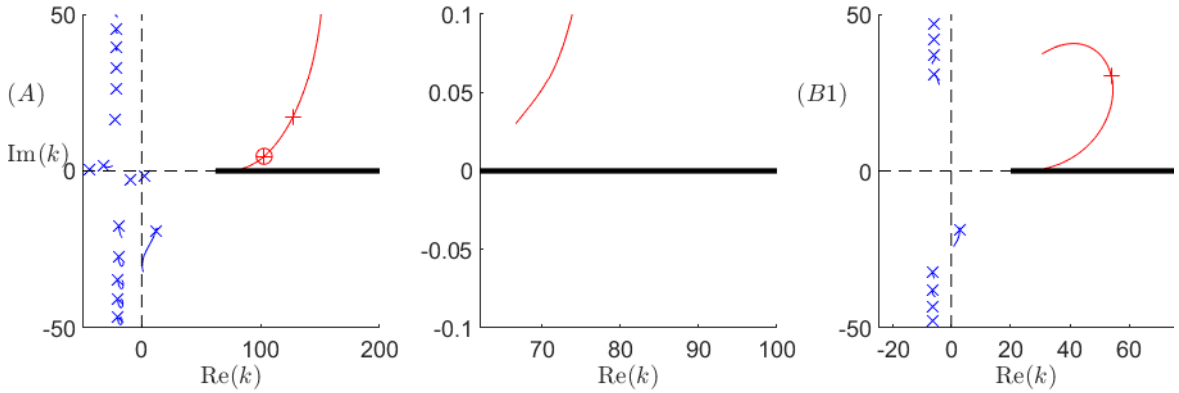

Fig. 12 Tracking of modal solutions in the complex k-plane for a linear shear flow profile as the boundary layer thickness, h, is varied, for parameter sets A and $B1$. The location of the hydrodynamic instability for parameter set A2 is marked with a circle.

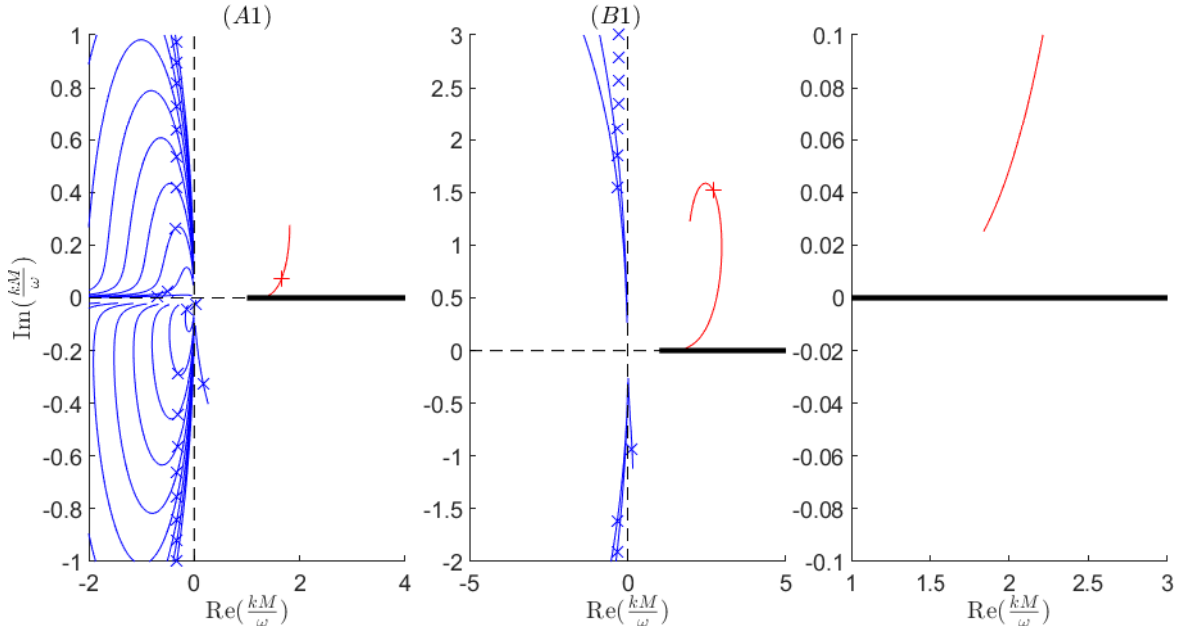

Fig. 13 Tracking of modal solutions in the rescaled complex k-plane for a linear shear flow profile as the centre line Mach number, M, is varied, for parameter sets A1, and B1.

remains exponential, although with a small exponent, and thus it will still dominate the far-field behaviour eventually, though it may be comparable in size within the near field. In contrast, for the linear flow profile we can instead find an additional stable modal pole located below the branch cut (and not behind the branch cut), that may move above and behind the branch cut as the parameters are varied, although this mode would then stop contributing instead of becoming unstable. This mode, when it is located below the branch cut, has a contribution that is exactly cancelled by the contribution of the critical layer branch cut, and so in all cases it does not contribute to the final Fourier inversion. For this reason it has not been included in our modal plots for the linear shear flow. It may additionally be observed that despite using the same parameter sets, when considering parameter set B we do have have two k_{HI} modes, as for the case of a quadratic shear flow, and again it is understood that we continue to have only one hydrodynamic instability in all cases.

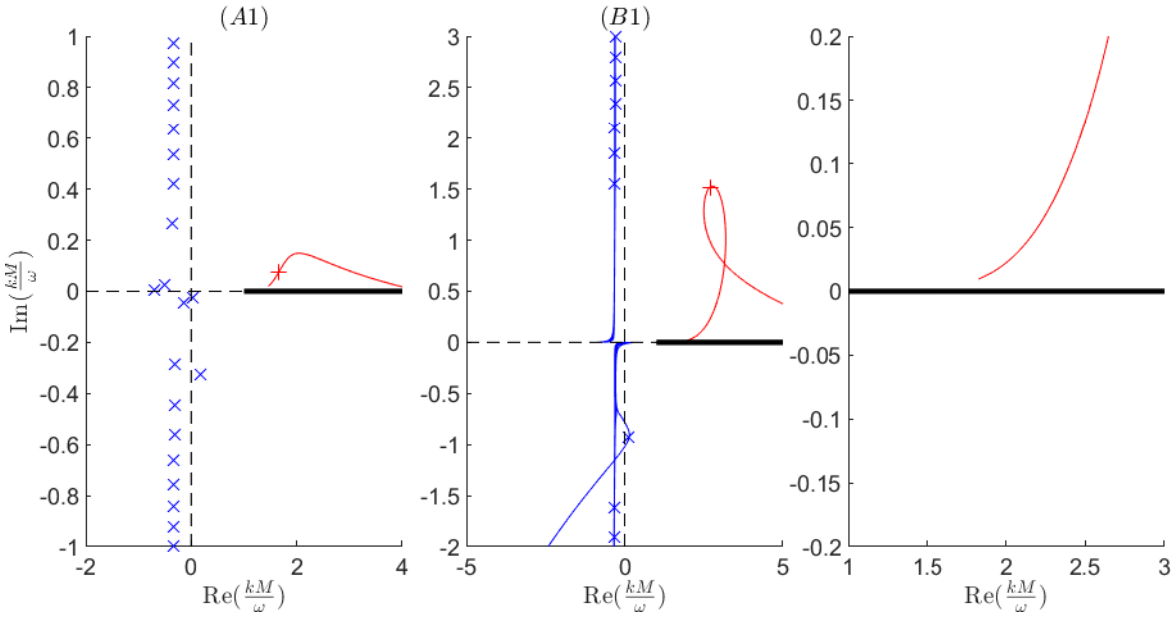

Fig. 14 Tracking of modal solutions in the rescaled complex k-plane for a linear shear flow profile as the frequency, ω, is varied, for parameter sets A1 (left), and B1 (middle and right). (right) a magnification near the critical layer branch cut for parameter set B1.

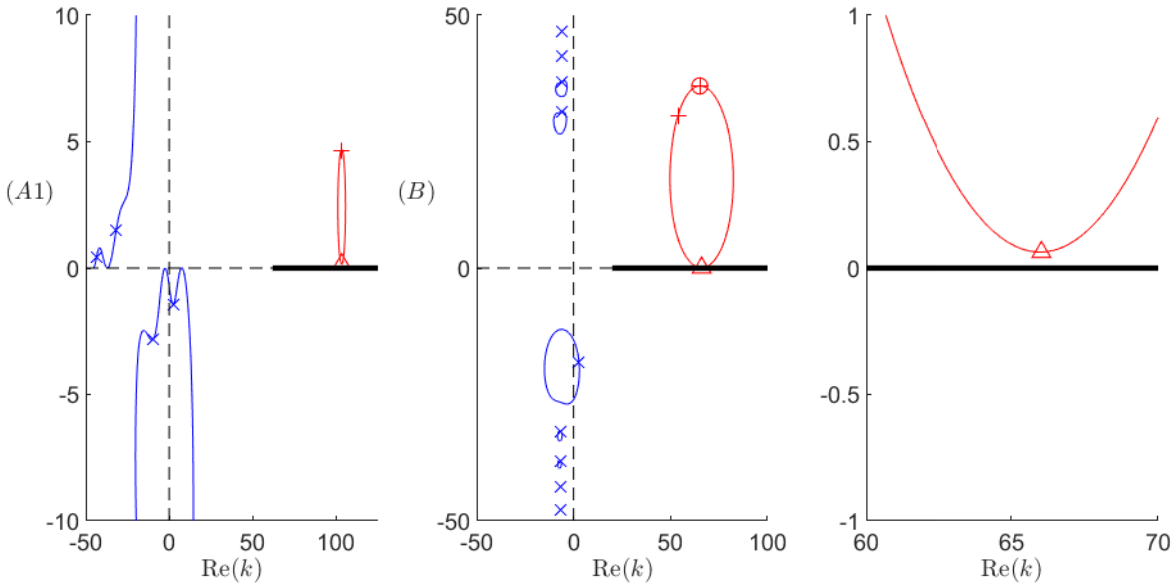

Fig. 15 Tracking of modal solutions in the complex k-plane for a linear shear flow profile as the imaginary part of the impedance, $\mathrm{Im}(Z)$, is varied, for parameter sets A1 and B, with a magnification of parameter set B near the critical layer branch cut (right). Behaviour at $|Z| = \infty$ is indicated by triangles ($\triangle$) for the hydrodynamic instability modes. Location of the hydrodynamic instability for parameter set B2 is circled.

IV. Conclusions

We have considered a cylindrical duct with a parallel mean flow that has a boundary layer that varies quadratically near the wall; we note again that this boundary layer need not be thin. The matlab code from [24] was used to solve for the modes using a Frobenius solution method, allowing the modes to be tracked through the critical layer branch cut. Modes behind the critical layer branch cut no longer appear in the modal sum, but still contribute to the overall solution through the Fourier inversion integral around the critical layer branch cut. From [24], it has already been shown that this can lead to the critical layer being the dominant contribution in the far-field downstream of a source, particularly when the source is located near the wall of the duct.

It has been observed that the hydrodynamic instability surface mode can be stabilized by its interaction with the critical layer. As has been observed previously [15], increasing the boundary layer thickness has a stabilizing effect. Here, we further find that increasing the boundary layer thickness can completely stabilize the flow by effectively removing the instability mode, which we have called k_{HI} throughout the main text, by hiding it behind the critical layer branch cut. We note that this mode was referred to as k^+ in [24].

The exact boundary layer thickness h_c required for the stabilisation of the k_{HI} mode varies depending on the Mach number, the frequency, and the impedance, and has been plotted in figures 6, 8 and 10 respectively. When varying the centre-line Mach number, lower Mach numbers lead to less instability, manifesting as a larger value of h_c. When varying the frequency, high- and low-frequencies are more stable, with often the hydrodynamic instability only being unstable for an intermediate range of frequencies. The mechanism behind the stabilization at high- and low-frequencies is however different, with high frequencies seeming to be innately stable, while low-frequencies are only more stable because of the spring-like impedance boundary. For a sufficiently thick boundary layer (depending on the parameters), the situation may be stable for all frequencies, which may be helpful for broadband time-domain simulations. When varying the impedance, the picture is complicated, as shown in figure 11. As the impedance tends to a hard wall, $|Z| \to \infty$, we find that $h_c \to 0$, implying that any thickness boundary layer over a hard wall is stable; while this is expected, it contrasts with the linear boundary layer profile which shows instability even as $|Z| \to \infty$. However, it should be noted that numerical difficulty with the Frobenius algorithm is found when $|k|$ becomes too large, which limits the values of parameters that may be searched, particularly for very small Mach numbers or near-hard walls.

This stabilisation by the critical layer found here for a quadratic boundary layer profile is in contrast to the constant-then-linear flow profile of [12], for which the hydrodynamic instability seems to always be unstable. Stabilization by the critical layer has also been observed in the case of a tanh boundary layer profile, using a finite difference method to track the mode into the branch cut as the impedance was varied. However, as this method could not analytically continue the solutions behind the branch cut, no further investigation could take place. Extending upon this, we believe this stabilisation behaviour will be typical of other sheared flow profiles; indeed, it was acknowledged in [12] that the critical layer in the linear boundary layer profile case is rather artificial, and is caused by the cylindrical duct geometry rather than the sheared mean flow, unlike in the quadratic case. It is therefore possible that extending the modified-Myers boundary condition, or other such uniform flow impedance boundary conditions, to account for a quadratic shear flow profile may reveal important details for correctly predicting the location of the hydrodynamic instability, which has previously been the least well-predicted mode.

Acknowledgments

M. J. King was supported in this work through the University of Warwick MASDOC Doctoral Training Centre, and gratefully acknowledges their support. E. J. Brambley gratefully acknowledges the support of the Engineering and Physical Sciences Research Council (EPSRC grant EP/V002929/1).

References

[1] Myers, M., "On the acoustic boundary condition in the presence of flow," *J. Sound Vib.*, Vol. 71, No. 3, 1980, pp. 429–434. doi:10.1016/0022-460X(80)90424-1.

[2] Brambley, E., "Fundamental problems with the model of uniform flow over acoustic linings," *J. Sound Vib.*, Vol. 322, No. 4-5, 2009, pp. 1026–1037. doi:10.1016/j.jsv.2008.11.021.

[3] Renou, Y., and Aurégan, Y., "Failure of the Ingard–Myers Boundary Condition for a Lined Duct: An Experimental Investigation," *J. Acoust. Soc. Am.*, Vol. 130, 2011, pp. 52–60. doi:10.1121/1.3586789.

[4] Brambley, E., "A Well-posed boundary condition for acoustic liners in straight ducts with flow," *AIAA J.*, Vol. 49, No. 6, 2011, pp. 1272–1282. doi:10.2514/1.J050723.

[5] Gabard, G., "A comparison of impedance boundary conditions for flow acoustics," *Journal of Sound and Vibration*, Vol. 332, No. 4, 2013, pp. 714–724. doi:10.1016/j.jsv.2012.10.014.

[6] Marx, D., and Aurégan, Y., "Effect of Turbulent Eddy Viscosity on the Unstable Surface Mode above an Acoustic Liner," *J. Sound Vib.*, Vol. 332, 2013, pp. 3803–3820. doi:10.1016/j.jsv.2013.02.005.

[7] Khamis, D., and Brambley, E., "Acoustics in a two-deck viscothermal boundary layer over an impedance surface," *AIAA J.*, Vol. 55, No. 10, 2017, pp. 3328–3345. doi:10.2514/1.J055598.

[8] Schulz, A., Weng, C., Bake, F., Enghardt, L., and Ronneberger, D., "Modeling of Liner Impedance with Grazing Shear Flow using a New Momentum Transfer Boundary Condition," AIAA paper, 2017-3377, 2017. doi:10.2514/6.2017-3377.

[9] Aurégan, Y., "On the use of a Stress–Impedance Model to describe Sound Propagation in a Lined Duct with Grazing Flow," *J. Acoust. Soc. Am.*, Vol. 143, No. 5, 2018, pp. 2975–2979. doi:10.1121/1.5037585.

[10] Weng, C., Schulz, A., Ronneberger, D., Enghardt, L., and Bake, F., "Flow and Viscous Effects on Impedance Eduction," *AIAA J.*, Vol. 56, No. 3, 2017, pp. 1118–1132. doi:10.2514/1.J055838.

[11] Spillere, A., Bonomo, L., Cordioli, J., and Brambley, E., "Experimentally Testing Impedance Boundary Conditions for Acoustic Liners with Flow: Beyond Upstream and Downstream," *J. Sound Vib.*, Vol. 489, 2020, p. 115676. doi:10.1016/j.jsv.2020.115676.

[12] Brambley, E., Darau, M., and Rienstra, S., "The critical layer in linear-shear boundary layers over acoustic linings," *J. Fluid Mech.*, Vol. 710, 2012, pp. 545–568. doi:10.1017/jfm.2012.376.

[13] Gabard, G., and Astley, R., "A computational mode-matching approach for sound propagation in three-dimensional ducts with flow," *Journal of Sound and Vibration*, Vol. 315, No. 4-5, 2008, pp. 1103–1124. doi:10.1016/j.jsv.2008.02.015.

[14] Yang, C., Fang, Y., Zhao, C., and Zhang, X., "On modeling the sound propagation through a lined duct with a modified ingard-myers boundary condition," *Journal of Sound and Vibration*, Vol. 424, 2018, pp. 173–191. doi:10.1016/j.jsv.2018.03.022.

[15] Rienstra, S. W., "Acoustic scattering at a hard–soft lining transition in a flow duct," *Journal of Engineering Mathematics*, Vol. 59, No. 4, 2007, pp. 451–475. doi:10.1007/s10665-007-9193-z.

[16] Jiang, H., Hong Lau, A. S., and Huang, X., "An efficient algorithm of Wiener–Hopf method with graphics processing unit for duct acoustics," *Journal of Vibration and Acoustics*, Vol. 139, No. 5, 2017. doi:10.1115/1.4036471.

[17] Sobolev, A., and Yakovets, M., "Application of the Wiener–Hopf method for describing the propagation of sound in cylindrical and rectangular channels with an impedance jump in the presence of a flow," *Acoustical Physics*, Vol. 63, No. 6, 2017, pp. 625–636. doi:10.1134/S1063771017060148.

[18] Briggs, R., "Criteria for Identifying Amplifying Waves and Absolute Instabilities," *Electron-Stream Interaction with Plasmas*, MIT, 1964, pp. 8–46. doi:10.7551/mitpress/2675.003.0004.

[19] Bers, A., "Space–time evolution of plasma instabilities — absolute and convective," *Basic plasma physics*, Vol. 1, edited by A. Galeev and R. Sudan, North-Holland, 1983, pp. 451–517.

[20] Rienstra, S., "A Classification of Duct Modes based on Surface Waves," *Wave Motion*, Vol. 37, 2003, pp. 119–135. doi:10.1016/S0165-2125(02)00052-5.

[21] Brambley, E., "Surface modes in sheared boundary layers over impedance linings," *J. Sound Vib.*, Vol. 332, No. 16, 2013, pp. 3750–3767. doi:10.1016/j.jsv.2013.02.028.

[22] Aurégan, Y., and Leroux, M., "Experimental Evidence of an Instability over an Impedance Wall in a Duct with Flow," *J. Sound Vib.*, Vol. 317, 2008, pp. 432–439. doi:10.1016/j.jsv.2008.04.020.

[23] Pridmore-Brown, D., "Sound propagation in a fluid flowing through an attenuating duct," *J. Fluid Mech.*, Vol. 4, No. 4, 1958, pp. 393–406. doi:10.1017/S0022112058000537.

[24] King, M., Brambley, E., Liupekevicius, R., Radia, M., Lafourcade, P., and Shah, T., "The critical layer in quadratic flow boundary layers over acoustic linings," , 2021. arXiv:2112.01643 (submitted for publication).

[25] Swinbanks, M., "The sound field generated by a source distribution in a long duct carrying sheared flow," *J. Sound Vib.*, Vol. 40, No. 1, 1975, pp. 51–76. doi:10.1016/S0022-460X(75)80230-6.